



Laser Ablation Molecular Isotopic Spectrometry: Parameter influence on boron isotope measurements

Xianglei Mao^a, Alexander A. Bol'shakov^b, Dale L. Perry^a, Osman Sorkhabi^a, Richard E. Russo^{a,*}

^a Lawrence Berkeley National Laboratory, University of California, Berkeley, CA 94720, USA

^b Applied Spectra, Inc., 46661 Fremont Boulevard, Fremont, CA 94538, USA

ARTICLE INFO

Article history:

Received 8 April 2011

Accepted 18 June 2011

Available online 30 June 2011

Keywords:

Optical isotopic measurement

Laser ablation plasma

Molecular emission spectra

LIBS

LAMIS of boron isotopes

Boron isotope

ABSTRACT

Laser Ablation Molecular Isotopic Spectrometry (LAMIS) was recently reported for optical isotopic analysis of condensed samples in ambient air and at ambient pressure. LAMIS utilizes molecular emissions which exhibit larger isotopic spectral shifts than in atomic transitions. For boron monoxide ^{10}BO and ^{11}BO , the isotopic shifts extend from 114 cm^{-1} (0.74 nm) to $145\text{--}238\text{ cm}^{-1}$ (5–8 nm) at the $B\ ^2\Sigma^+ (v=0) \rightarrow X\ ^2\Sigma^+ (v=2)$ and $A\ ^2\Pi_1 (v=0) \rightarrow X\ ^2\Sigma^+ (v=3)$ transitions, respectively. These molecular isotopic shifts are over two orders of magnitude larger than the maximum isotopic shift of approximately 0.6 cm^{-1} in atomic boron. This paper describes how boron isotope abundance can be quantitatively determined using LAMIS and how atomic, ionic, and molecular optical emission develops in a plasma emanating from laser ablation of solid samples with various boron isotopic composition. We demonstrate that requirements for spectral resolution of the measurement system can be significantly relaxed when the isotopic abundance ratio is determined using chemometric analysis of spectra. Sensitivity can be improved by using a second slightly delayed laser pulse arriving into an expanding plume created by the first ablation pulse.

© 2011 Elsevier B.V. All rights reserved.

1. Introduction

Laser Ablation Molecular Isotopic Spectrometry (LAMIS) was recently reported for real-time isotopic analyses of samples at ambient pressure [1]. LAMIS involves the generation of a laser induced plasma and measurement of molecular spectra of the radicals that are produced following ablation into the atmosphere. The traditional approach to using optical emission spectrometry in laser ablation plasma is known as Laser-Induced Breakdown Spectroscopy (LIBS), which is primarily used for elemental analysis of condensed phase samples using atomic spectroscopy [2–6]. In a number of previous studies, some molecular emissions were used for laser induced plasma diagnostics [7,8] and as additional spectral features in LIBS applications for identifying organic materials (pathogenic bacteria, explosive residues, biological and chemical agents) [9,10]. Quantitative analytical LIBS measurements using molecular emission at atmospheric pressure have been only recently demonstrated on complex organic matrices [11].

The benefits of laser plasma spectrometry are well established; real-time elemental analysis at atmospheric pressure, no sample preparation, and no consumables. The technology can be used in a laboratory or field environment for contact and open-path stand-off measurements [10,12–14]. Nevertheless, laser plasma spectrometry is

generally not utilized as a source for isotope detection for the following reasons: (1) broadening of spectral lines due to Stark and Doppler effects, and (2) relatively small isotope splitting for atomic species. For example, the isotopic shift for ^{10}B and ^{11}B atomic resonant transition at 208.9 nm is only 2.5 pm, while Stark broadening of this line in typical LIBS plasmas can be larger than 100 pm. ^{235}U and ^{238}U have an isotopic shift of 25 pm for the ionic emission line at 424.4 nm. For the plutonium isotopes ^{239}Pu and ^{240}Pu , the isotopic shift is 12 pm for the emission line at 594.5 nm.

There are several proven ways to overcome these challenges: (1) performing laser ablation with the sample in vacuum or noble gas environments [15–18], (2) using plasma sources – such as ICP (inductively coupled plasmas) – that have lower electron number densities [19–21], (3) using chemometric analysis [22], and now, using LAMIS [1]. Recent work at the National Research Council in Canada demonstrated that a relatively low resolution spectrometer was able to measure the $^{235}\text{U}/^{238}\text{U}$ ratio at 424.4 nm using chemometric analysis of the spectra from a laser plasma at atmospheric pressure [22]. Isotope measurements using optical emission have been reported in other plasma sources that have lower electron density than the laser plasma [19–21]. For example, the electron number density in ICP is typically $\sim 10^{15}\text{ cm}^{-3}$ compared to $\sim 10^{17}\text{ cm}^{-3}$ in the laser ablation plasmas used in LIBS. Hence, a high-resolution spectrometer was able to resolve the uranium isotopes of 233, 235, 236 and 238 at the same 424.4 nm electronic transition in ICP [23]. These studies relied on the electronic transition of the ionized uranium atom that has a relatively large 235/238 isotopic shift of 25 pm. Isotopic shifts for other elements

* Corresponding author.

E-mail address: rerusso@lbl.gov (R.E. Russo).

are commonly only a few picometers [24]. LAMIS on the other hand is based on the measurement of molecular emission bands in the laser plasma which exhibit large isotopic splitting due to contributions of the rotational and vibrational states of the molecule. For ^{10}B and ^{11}B , we predicted and measured an isotopic shift of 744 pm (114 cm^{-1}) in the BO emission band (0,2) $\text{B} \rightarrow \text{X}$ at 255–256 nm; more than two orders of magnitude greater than the isotopic splitting of 2.5 pm (0.57 cm^{-1}) in the atomic boron prominent line at 208.89 nm.

Boron and its isotopes are emphasized in this work because of the significance of boron in a number of analytical and technical disciplines. Coatings enriched in ^{10}B are widely used in the materials sciences of neutron detection materials [25–28], since neutron capture cross section of ^{10}B is six orders of magnitude higher than that of ^{11}B and significantly higher than that of any other materials. Owing to such unique nuclear properties, natural and isotope-enriched boron is often utilized as neutron shielding and neutron absorbing materials in nuclear reactors. Isotopic boron also has wide applications in medical technology, with one major application of neutron capture therapy [29,30]. Boron isotopes are the centerpiece for the entire field of boron nuclear magnetic resonance (^{10}B and ^{11}B NMR) spectroscopy and magnetic resonance imaging diagnostics [31–33]. Boron ingredients have been shown necessary for both human and animal nutrition [34,35]. Boron also is the basis for several major areas of materials chemistry, including boranes [36], amine-boranes [37], and elemental borides [33,38].

LAMIS extends the previously established advantages of LIBS technology into the new field of isotopic analysis. Using commercial LIBS instruments [39,40] with a technique of LAMIS, one can rapidly scan over either surface or depth distributions of a specific isotope in any material, structure or tissue with lateral resolution of $\sim 50\text{ }\mu\text{m}$ and depth resolution of $\sim 20\text{ nm}$. The nominal sample quantity can be less than $1\text{ }\mu\text{g}$. Three-dimensional isotopic mapping with fine spatial resolution is necessary in boron radio-chemotherapeutic cancer research, in which neutron capture by ^{10}B -loaded targeted drugs generate lethal radiation that damages DNA within individual malignant cells. Presently, isotopic mapping at the scale of tens of microns can be obtained with laser ablation – inductively coupled plasma – mass spectrometry (LA-ICP-MS) or secondary ion mass spectrometry (SIMS), both involving large and expensive instrumentation. In contrast, LAMIS can be implemented as a fieldable device. Application of LAMIS for localized boron isotope determination is of interest in the development of handheld semiconductor-based neutron sensors, in which a layer of ^{10}B -enriched boron carbide with thickness of 1.5 to $100\text{ }\mu\text{m}$ is deposited on top of a regular silicon-based diode [28]. Other neutron detection devices lined, coated or loaded with ^{10}B can be rapidly tested by LAMIS for isotopic and elemental composition, hetero- or homogeneity, and possible defects for the purpose of quality assessment and quality control. In nuclear reactors with boron neutron capture or boric acid added coolants, the ability to measure the ^{10}B and ^{11}B content by LAMIS will be particularly useful. By analogy with LIBS [41], such monitoring can be achieved remotely through a small window.

Because of the importance of boron in research, its chemistry and materials science aspects, and technology in a number of fields, LAMIS should play an important role in the general analytical chemistry of the element and in research of boron with respect to isotope-based experiments. LAMIS can be applicable in studies where different isotopes are used as tracers during reaction chemistry and also for monitoring the feedstock or analyzing the reaction products that can be in bulk as well as in thick or thin films. Isotope exchange reactions, interfacial reactions involving fluids, and studies of solid state interfaces of boron materials are but a few types of experiments.

This manuscript reports quantitative results for boron isotopic analysis using LAMIS. Also discussed are the effects of acquisition delay time on the measurement of boron monoxide in the laser plasma, measurement and calibration of standard samples with

known $^{10}\text{B}/^{11}\text{B}$ isotope ratios using partial least squares (PLS) regression, and the influence of spectral resolution on the prediction of abundance ratio. Application of two closely successive laser pulses (a double-pulse approach) is shown to improve sensitivity.

2. Experimental

Samples with known boron isotopic ratio were ablated using a Nd:YAG laser with a wavelength of 1064 nm, pulse energy of 50–100 mJ, and a pulse duration of 4 ns. The laser beam was focused onto the sample with a quartz lens to a spot diameter of $\sim 100\text{ }\mu\text{m}$. A second lens was used to collect the laser-induced plasma emission onto the entrance of a fiber optic cable coupled to a Czerny-Turner spectrometer with an Intensified Charge-Coupled Device (ICCD). The signal acquisition delay after the laser pulse was varied to demonstrate the relative intensities for atomic, ionic and molecular emission. The spectra represent accumulation of single or multiple laser pulses; the number of pulses for each measurement is noted in figure captions. Additional measurements were performed at different spectral resolution by changing the entrance slit width of the spectrometer. The spectral resolution is determined by measuring the full width at half maximum (FWHM) of the Hg line. All measurements were performed in air at atmospheric pressure.

A double-pulse LAMIS setup consisted of two lasers and a detection system. The wavelength of the ablation laser was 355 nm, and its pulse energy 8.5 mJ. The second laser's wavelength was 1064 nm with pulse energy 75 mJ. The second laser propagated orthogonal to the first ablation laser. The time delay between the two laser pulses was $2.4\text{ }\mu\text{s}$. The second laser pulse was focused inside the first laser induced plasma at a height approximately 1 mm above the sample surface. The ICCD acquired spectra at $8\text{ }\mu\text{s}$ delay after the ablation laser. The gated acquisition time was 30 μs .

Boron nitride (BN) pressed-powder disks with natural isotopic abundance were used as samples. These BN disks were commercial sputtering targets designed for film deposition in the electronics and optical industry (obtained from Alfa Aesar, 99.99% purity). Additionally, isotope-enriched samples of $^{10}\text{B}_2\text{O}_3$ and $^{11}\text{B}_2\text{O}_3$ (99% ^{10}B and 95% ^{11}B) were used as reference standards. The boron oxide samples were purchased from Cambridge Isotope Laboratories, Inc. (Andover, MA, USA). To prepare the different isotope ratio boron oxide reference samples, we mixed different amounts of isotope-enriched B_2O_3 and pressed them with 7 ton pressure for 4 min into one-centimeter diameter pellets.

3. Results and discussion

We demonstrated that isotopic shifts can be orders of magnitude larger in molecular versus atomic optical emission [1]. In LAMIS, an ablating laser pulse is impinging on the sample surface that results in explosive vaporization, atomization and partial ionization of matter from the sample and surrounding air. After the plasma in a plume cools down sufficiently, the molecular radicals form. In particular, the diatomic oxide radicals form when atoms evaporated from the sample react with dissociated atmospheric oxygen. A small deviation in plasma chemistry of different isotopes of the same element may occur but in general, all isotopes undergo very similar reactions. Quantitative calibration then relates the measured spectra of isotopomeric radicals in an ablation plume to the original abundances of isotopes in the sample.

In the first experiment, a BN sample was ablated with an infrared Nd:YAG laser. The ejected boron atoms reacted with oxygen from air and formed BO radicals in a laser ablation plume. The spectra in Fig. 1 show the laser plasma optical emission spectra of the boron monoxide transition $\text{B } ^2\Sigma^+ (v=0) \rightarrow \text{X } ^2\Sigma^+ (v=2)$ in the wavelength region of 255 to 259 nm. In Fig. 1a, the black and red traces are the simulated emission spectra of $^{11}\text{B}^{16}\text{O}$ and $^{10}\text{B}^{16}\text{O}$, respectively. This simulation

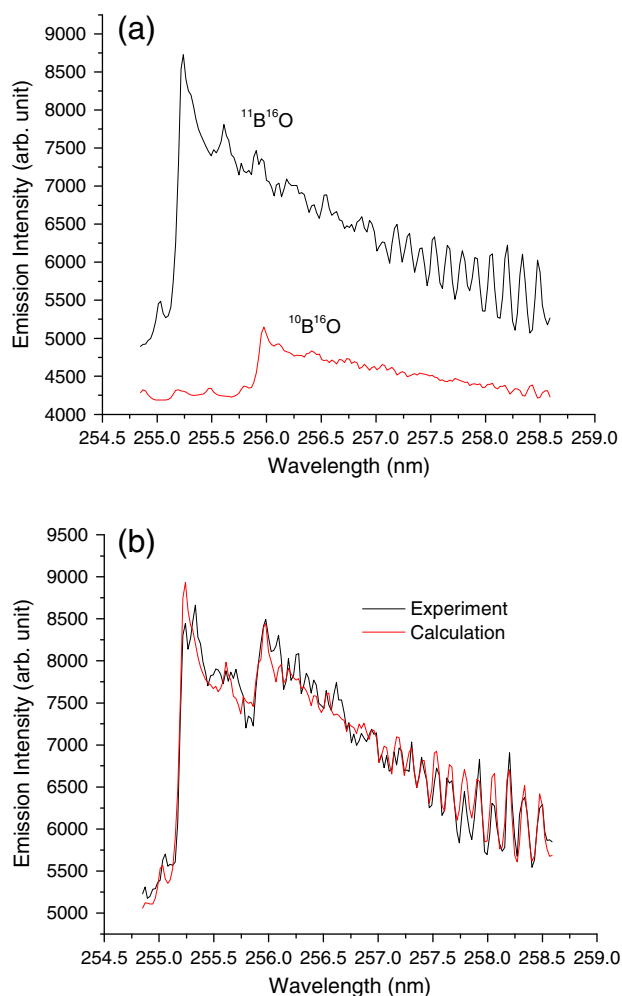


Fig. 1. Experimental and simulated emission spectra of boron monoxide, BO. (a) The black and red traces are the simulated emission spectra of ^{11}BO and ^{10}BO , respectively. (b) The black spectrum represents the measured spectrum with natural isotopic abundance of boron accumulated from 100 laser pulses; the red trace is a sum of simulated ^{11}BO and ^{10}BO spectra with a fitted abundance of 20.24% for ^{10}BO . The spectral resolution is 70 pm.

included a natural isotopic abundance factor of 80.2% and 19.8% for ^{11}B and ^{10}B , respectively. In Fig. 1b, the black and red traces correspond respectively to the experimentally measured spectrum and to a combined sum of both simulated isotopic spectra from Fig. 1a. The spectrometer resolution used in these measurements was 70 pm. The band head isotopic shift of ~ 740 pm is easily observed at atmospheric pressure for this spectral emission. In contrast, the isotopic shift for atomic boron emission at 208.9 nm is only 2.5 pm; almost three hundred times smaller than in the $\text{B} \rightarrow \text{X}$ transition of BO. Among other atomic boron transitions, the line at 208.9 nm has one of the largest known isotopic shifts in B on the scale of energy or wave numbers (0.57 cm^{-1}). The only one other boron line at 821.2 nm has slightly larger isotopic shift of 0.61 cm^{-1} [42]; such small shifts in atomic spectral lines cannot be easily resolved at atmospheric pressure.

The simulations of boron monoxide spectra presented in Fig. 1 were performed as previously described [1]. The laser plasma at long delays after the laser pulse was assumed to reach local thermodynamic equilibrium (LTE) with a uniform and quasi-steady-state temperature of 5000 K. The minor differences in the measured (black) and simulated (red) spectra discernible in Fig. 1b can occur due to possible inaccuracy in molecular constants which we have used

[43], and also due to neglected plasma kinetics and gradients in temperature that actually drops in time. If more accurate molecular spectral simulations were available and a kinetic plasma model was applied, we would be able to further address the non-equilibrium nature of the plasma that can cause measurable differences in the spectra. However, we achieved a reasonable agreement between experimental and simulated spectra using a regular steady-state LTE model. The latter fact justifies our simple initial assumptions.

Thus, we calculated the abundance of the minor boron isotope by fitting the simulated $\text{B} \rightarrow \text{X}$ emission of BO to the experimental spectra. The abundance of ^{10}B was determined as 20.2% from this LAMIS spectrum by using a least squares fitting technique. The value is within the ^{10}B natural abundance range of 19.3% to 20.2% (with the mean of 19.8%) [44]. An estimated detection limit for the minor ^{10}B isotope was approximately 1% as directly measured in our solid boron nitride sample. Even if the ablated sample was boron nitride, no BN molecular emission was observed in the range of 200–900 nm. More accurate molecular constants, if available and a more sophisticated modeling of plasma conditions and molecular formation can possibly improve the fit and accuracy of the isotope abundance determination. A different approach to determine the isotopic concentration is described later in this work.

The data in Fig. 2 show how atomic, ionic, molecular and continuum emission evolve with time in the laser plasma; the behavior is specific to the conditions (laser energy, energy density, pulse duration) used in these experiments. The intensity scale in this figure is normalized to the ICCD gate width and the number of accumulated signal acquisitions. As generally known and as measured here, atomic emission persists longer than ionic; and molecular emission increases after the atomic and ionic begin to decrease. Molecular emission can persist for tens of microseconds after the laser pulse. Accurate measurements of molecular emission are facilitated by the fact that a plasma continuum background drops rapidly at long delays, making feasible the registration of molecular emission with an extended acquisition gate width.

Molecular emission in these experiments was measured later than $\sim 1 \mu\text{s}$ after the ablating laser pulse because of high continuum background fluctuations at earlier times. Temporal behavior of two resolved molecular lines is displayed in Fig. 2: one measured at

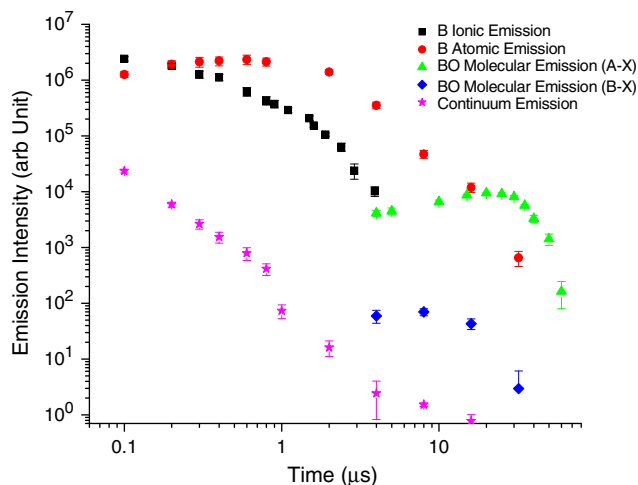


Fig. 2. Emission intensities of boron atomic and ionic lines, boron monoxide lines and continuum radiation versus delay time from the moment of laser ablation. ICCD gate width was the same as the delay but the presented data was normalized by the gate width and the number of accumulated spectra. Black squares for the intensity of boron ionic line at 345.13 nm; red circles for the boron atomic line at 249.77 nm; green triangles for the BO molecular emission at 572 nm (0,3 band of A \rightarrow X); blue diamonds for the BO molecular emission at 256 nm (0,2 band of B \rightarrow X); and stars for the continuum background radiation at 255 nm.

255 nm corresponding to an individual rotational line of the BO transition $B^2\Sigma^+ (v=0) \rightarrow X^2\Sigma^+ (v=2)$, and the other measured at 572 nm corresponding to an individual rotational line of the $A^2\Pi_i (v=0) \rightarrow X^2\Sigma^+ (v=3)$ transition. These two particular rotational lines were chosen because they are well-resolved from other features in the spectra. The emission at 572 nm of the $A \rightarrow X$ transition is approximately two orders of magnitude more intense than the emission at 255 nm of the transition $B \rightarrow X$ (Fig. 2). This fact indicates that the lower electronic states of BO molecules are more populated than the higher excited states of BO in the laser plasma. The upper energy level (T_e) of the $B^2\Sigma^+$ state is 43173 cm^{-1} , and that of the $A^2\Pi_i$ is 23897 cm^{-1} . The emission intensity is proportional to the exponential function of upper energy level over temperature in accordance with the Boltzmann distribution.

As expected, the emission intensities of individual molecular rotational lines are weaker than intensities of the prominent spectral lines (249.77 and 345.13 nm in Fig. 2) of neutral and ionized boron atoms. However, if the overall intensity of the BO molecular bands was spectrally integrated, then the collective molecular intensity (e.g., unresolved, summed up) would be comparable to the intensity of atomic and ionic emissions. In the present study, no such spectral integration of the molecular spectra was performed. While molecular emission intensified with time, the continuum radiation level decreased more than 1000 times in the plasma from 1 to 32 μs . From the measurements presented in Fig. 2, we chose a fixed gate width of 30 μs and a gate delay of 4 μs after the laser pulse for the subsequent quantitative measurements of isotopic concentrations.

The calculated isotopic shifts between $^{10}\text{B}^{16}\text{O}$ and $^{11}\text{B}^{16}\text{O}$ band origins for the $B^2\Sigma^+ \rightarrow X^2\Sigma^+$ and $A^2\Pi_i \rightarrow X^2\Sigma^+$ transitions are listed in Table 1. Calculations of the shifts for several vibrational bands in the spectra of ^{10}BO and ^{11}BO were performed following Ref. [1], Eq. 3 within Herzberg's framework of molecular spectra [45]. The simulated BO spectra indicated that the isotopic shift at the band origin of the transition $A^2\Pi_i (v=0) \rightarrow X^2\Sigma^+ (v=3)$ should be 165 cm^{-1} (5 nm). With the rotational quantum number about $J=50$ in the tail of this (0,3) vibrational band at the wavelength around 580 nm, the isotopic

shift will be $200\text{--}240 \text{ cm}^{-1}$ (7–8 nm) depending on the divergence between the P, Q and R branches (see Ref. [1], Eq. 4).

We performed multivariate calibration using reference samples with known isotopic ratio. The spectral interval of 579–585 nm was chosen because a significant difference in the spectra of ^{10}BO and ^{11}BO isotopomeric radicals was clearly observed in this wavelength region (Fig. 3). The spectrometer resolution was initially set at 20 pm. Spectra were recorded after each ablating laser pulse and then averaged over 100 measurements. Several vertical dashed lines in Fig. 3 indicate the wavelength positions at which the differences between ^{10}BO and ^{11}BO spectra are the most apparent.

We prepared several mixtures of the two enriched samples of $^{10}\text{B}_2\text{O}_3$ and $^{11}\text{B}_2\text{O}_3$ (99% ^{10}B and 95% ^{11}B) and used them as reference standards for quantitative calibration. These mixtures with known boron isotopic abundances were ($^{10}\text{B}_{0.99}\text{ }^{11}\text{B}_{0.01}$) $_2\text{O}_3$, ($^{10}\text{B}_{0.8}\text{ }^{11}\text{B}_{0.2}$) $_2\text{O}_3$, ($^{10}\text{B}_{0.52}\text{ }^{11}\text{B}_{0.48}$) $_2\text{O}_3$, ($^{10}\text{B}_{0.05}\text{ }^{11}\text{B}_{0.95}$) $_2\text{O}_3$. Boron nitrite of natural isotope abundance ($^{10}\text{B}_{0.2}\text{ }^{11}\text{B}_{0.8}$)N was also used as a standard.

We used a PLS linear regression routine to match a spectrum of the unknown sample to one of the reference spectra. We applied this PLS routine as a progressive approach to obtain multivariate calibration that takes into account all intensities at every pixel within the region 579–585 nm, as opposed to traditional univariate calibration that is built using only one pre-selected spectral line (or other single spectral feature) at a specific wavelength. The multivariate approach is more accurate, robust and reliable in comparison to univariate calibration. Multivariate calibration can be performed correctly even when spectra are only partially resolved. The later aspect is particularly important for molecular spectra.

Table 1

The calculated isotopic shifts in band origins of molecules $^{10}\text{B}^{16}\text{O}$ and $^{11}\text{B}^{16}\text{O}$. Only the bands experimentally observed in LAMIS are listed.

Transition	v'	v''	Wave number (cm^{-1})	Wavelength (nm)	Isotope shift $-1 \times (\text{pm})$	Isotope shift (cm^{-1})
$B^2\Sigma^+ - X^2\Sigma^+$	0	1	41011	243.765	369	62
	0	2	39172	255.207	744	114
	0	3	37357	267.608	1181	165
	1	0	44133	226.518	-140	-27
	1	1	42271	236.497	146	26
	1	3	38617	258.873	864	129
	1	4	36826	271.470	1313	178
	2	1	43510	229.761	-45	-9
	2	2	41672	239.899	250	43
	3	1	44728	223.505	-210	-42
	3	2	42889	233.087	54	10
	$A^2\Pi_i - X^2\Sigma^+$	0	1	21723	460.210	1323
0		2	19885	502.761	2895	114
0		3	18069	553.265	5056	165
1		0	24823	402.731	-426	-26
1		1	22962	435.389	515	27
1		2	21123	473.285	1774	79
2		0	26039	383.924	-888	-60
3		0	27233	367.096	-1253	-93
4		0	28404	351.958	-1540	-124
5		0	29553	338.276	-1766	-154
6	0	30680	325.855	-1944	-183	

Isotopic shifts were calculated following Ref. [1], Eq. 3 giving an opposite sign for the shifts in wavelength and those in wave numbers. Wave numbers were calculated using the energy terms difference $T_e(v') - T_e(v'') + G(v') - G(v'')$. Molecular constants were taken from Ref. [43]. BO isotope mass coefficient $\rho = 1.029$ was used. The wave numbers are in vacuum; the wavelengths are in air.

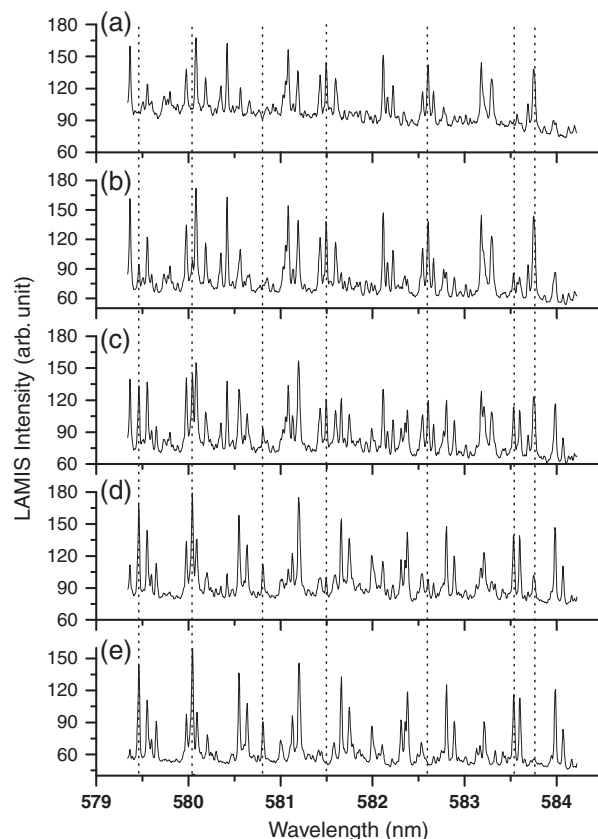


Fig. 3. BO spectra from samples of different boron isotope concentration. (a) $^{10}\text{B}_{0.99}\text{ }^{11}\text{B}_{0.01}\text{O}$, (b) $^{10}\text{B}_{0.8}\text{ }^{11}\text{B}_{0.2}\text{O}$, (c) $^{10}\text{B}_{0.52}\text{ }^{11}\text{B}_{0.48}\text{O}$, (d) $^{10}\text{B}_{0.2}\text{ }^{11}\text{B}_{0.8}\text{O}$, and (e) $^{10}\text{B}_{0.05}\text{ }^{11}\text{B}_{0.95}\text{O}$. The vertical dashed lines indicate the wavelength positions at which the differences between ^{10}BO and ^{11}BO spectra are the most apparent.

In order to compile a library of reference spectra for the multivariate PLS calibration, we recorded 100 separate spectra from each reference sample (without averaging). Each spectrum was from a single laser pulse. Using these spectra, we calculated a PLS regression coefficient matrix that correlated boron isotopic abundance to the relevant reference spectra, which included information on their pulse-to-pulse variability. In this fashion, we obtained linear calibration for concentrations of the major boron isotope ^{11}B in a sample to be analyzed (Fig. 4). The error bars correspond to standard deviations recorded in a series of 100 single-shot measurements. Excellent linear relationship was obtained in this calibration graph with a correlation coefficient very close to unity $r=0.9993$.

The established relationship linked to the library of spectra provides a means to determine ^{11}B concentration in unknown samples. Determination is realized by collecting a boron monoxide spectrum (or repetitive spectra) in laser ablation of an unknown sample, and then applying the pre-computed PLS coefficient matrix. The PLS regression yields a predicted ^{11}B concentration in the sample. For example, we used the BN disk sample as “unknown” to collect another 100 ablation spectra. Concentration of ^{11}B in the BN sample of natural abundance was determined as $(78 \pm 3.7)\%$, which compares favorably with the known average isotopic abundance of 80.2%. This approach to isotopic determination is fully empirical and does not require simulation of the spectra or plasma state assumptions.

The large isotopic spectral shift in molecular transitions observed in this work relaxes requirements on resolution of the spectrometer. In order to investigate the effect of spectral resolution, we varied the resolution of our spectrometer from 20 pm to 230 pm (Fig. 5). As shown in Fig. 6, calibration (built using the same PLS routine as described earlier and established from the series of 100 single pulse spectra) did not change within an experimental standard relative deviation of $\sim 3.5\%$. All data with varied resolution combined together resulted in a value of $(79.6 \pm 2.8)\%$ of ^{11}B isotope abundance in the BN sample, that is in agreement with the natural abundance range of 79.8% to 80.7% [44]. Therefore, high-resolution spectrometers are not necessary for the quantitative LAMIS measurements. Ability to measure isotope abundance with a low resolution spectrometer is a significant attribute of LAMIS.

The double-pulse approach, in which a second laser pulse is coupled into a laser plasma with a short delay after the first pulse, has been shown to increase atomic and ionic emission [10,46]. Similar enhancements were measured for molecular emission as shown in Fig. 7. The ablated mass in both double-pulse and single-pulse measurements was the same. Therefore, enhancement in intensity of molecular spectra can be attributed to higher electronic and

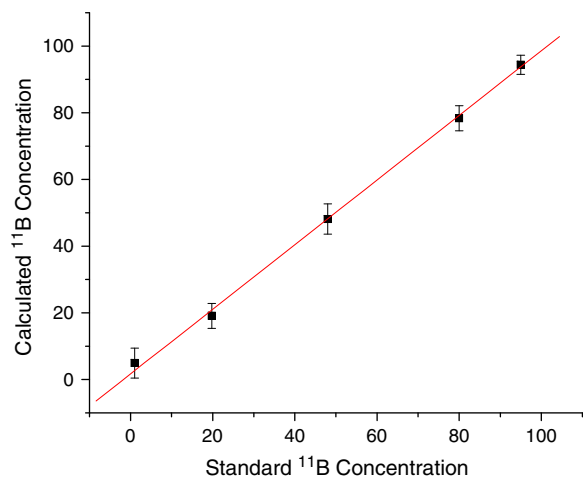


Fig. 4. Concentration of ^{11}B predicted by PLS calibration of the LAMIS spectra versus known ^{11}B concentration in the reference samples.

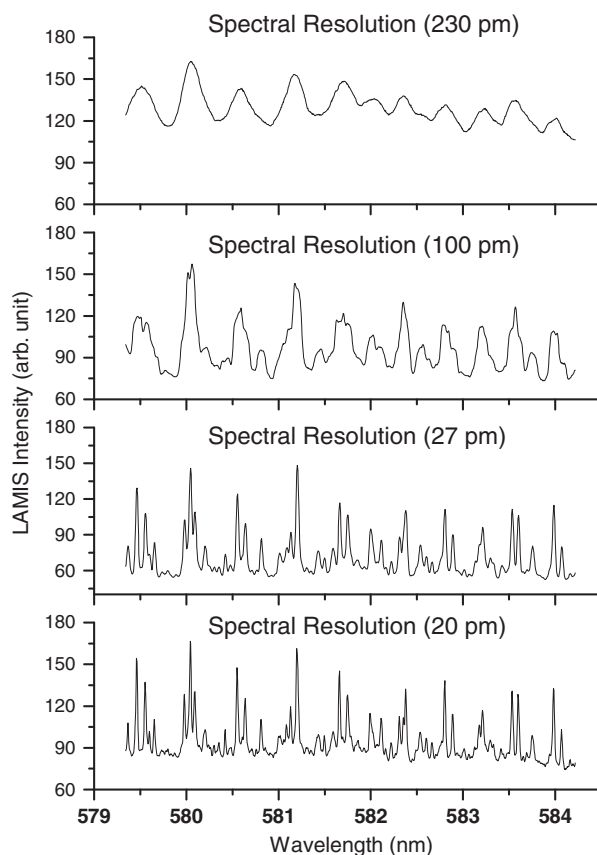


Fig. 5. BO emission spectra from laser ablation of BN sample measured with different spectral resolution (20, 27, 100, and 230 pm). Delay 4 μs , gate width 30 μs .

collisional excitation of molecules in the double-pulse approach. Optimization of delay time and relative pulse energy need to be established to determine how such enhancements influence sensitivity and precision performance. However, it is clear from these data that sensitivity can be increased.

4. Conclusion

Large isotopic shifts from 0.74 up to 5–8 nm in emission spectra of ^{10}BO and ^{11}BO molecular radicals were measured. These spectra were used for the rapid isotopic analysis of BN and B_2O_3 samples at

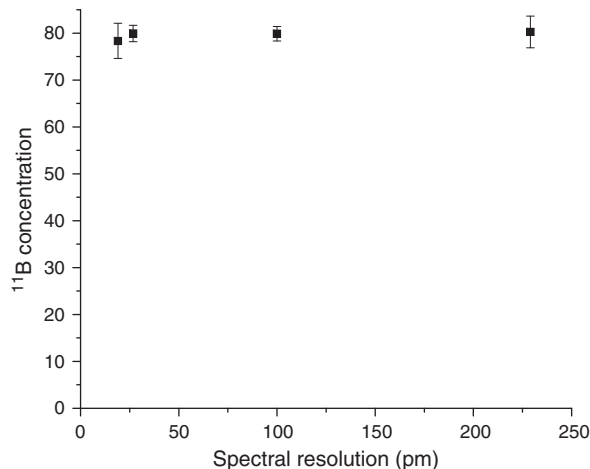


Fig. 6. Concentration of ^{11}B in the BN sample as predicted by PLS calibration versus spectral resolution of the recording spectrometer.

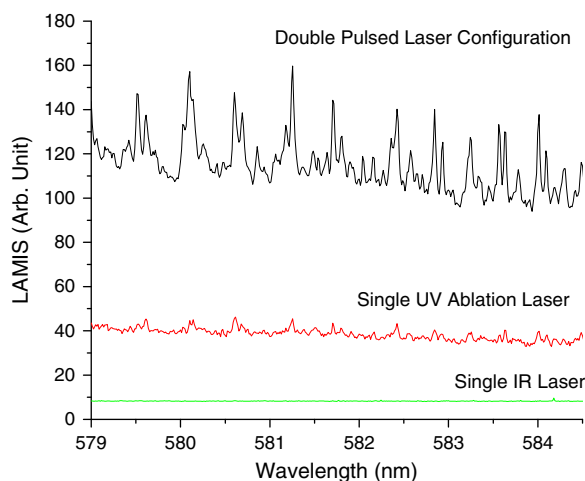


Fig. 7. BO emission spectra from laser ablation of the BN sample measured in the double-pulse scheme. The green trace shows the effect of firing the second laser without the first ablation pulse. The red spectrum corresponds to single laser pulse ablation. The black spectrum corresponds to application of the two laser pulses separated by 2.4 μ s: emission enhanced by additional heating of laser plasma. All data recorded accumulating 100 spectra.

atmospheric pressure. Quantitative determination of boron isotopes in laser ablation plasmas was performed using two different approaches, both of which yielded accurate results. High spectral resolution of molecular spectra was not required for quantitative calibration of the LAMIS technique. The dynamic range of isotopic quantification was from \sim 1% to 100% in boron-containing solid samples. Double pulse and other plasma heating methods have been found to enhance S/N for achieving lower detection limits.

Acknowledgment

This work was supported by the Defense Threat Reduction Administration (DTRA) of the U. S. Department of Defense under Federal Awards No. LB09005541 and LB09005541A, and Contract no. DE-AC02-05CH11231 awarded by the U.S. Department of Energy through the National Nuclear Security Administration (NNSA); and NASA Contract no. NNX10CA07C awarded to Applied Spectra Inc.

References

- [1] R.E. Russo, A.A. Bol'shakov, X. Mao, C.P. McKay, D.L. Perry, O. Sorkhabi, Laser ablation molecular isotopic spectrometry, *Spectrochim. Acta Part B* 66 (2011) 99–104.
- [2] D.M. Wong, A.A. Bol'shakov, R.E. Russo, Laser induced breakdown spectroscopy, in: J. Lindon, G. Tranter, D. Koppenaal (Eds.), *Encyclopedia of Spectroscopy and Spectrometry*, 2nd Edition, Academic Press, 2010, pp. 1281–1287.
- [3] J.P. Singh, S.N. Thakur (Eds.), *Laser-Induced Breakdown Spectroscopy*, Elsevier, Amsterdam, Oxford, 2007.
- [4] D.A. Cremers, L.J. Radziemski, *Handbook of Laser-Induced Breakdown Spectroscopy*, J. Wiley & Sons, New York, 2006.
- [5] A.W. Miziolek, V. Palleschi, I. Schechter (Eds.), *Laser-Induced Breakdown Spectroscopy (LIBS), Fundamentals and Applications*, Cambridge University Press, UK, 2006.
- [6] Y.-I. Lee, K. Song, J. Sneddon, *Laser-Induced Breakdown Spectroscopy*, Nova Science Publishers, Huntington, NY, 2000.
- [7] C.G. Parigger, G. Guan, J.O. Hornkohl, Measurement and analysis of OH emission spectra following laser-induced optical breakdown in air, *Appl. Opt.* 42 (2003) 5986–5991.
- [8] C.G. Parigger, J.O. Hornkohl, A.M. Keszler, L. Nemes, Measurement and analysis of atomic and diatomic carbon spectra from laser ablation of graphite, *Appl. Opt.* 42 (2003) 6192–6198.
- [9] J. Diedrich, S.J. Rehse, S. Palchadhuri, Pathogenic *Escherichia coli* strain discrimination using laser-induced breakdown spectroscopy, *J. Appl. Phys.* 102 (2007) 014702.
- [10] J.L. Gottfried, F.C. De Lucia, C.A. Munson, A.W. Miziolek, Double-pulse standoff laser-induced breakdown spectroscopy for versatile hazardous materials detection, *Spectrochim. Acta Part B* 62 (2007) 1405–1411.

- [11] F.R. Doucet, P.J. Faustino, M. Sabsabi, R.C. Lyon, Quantitative molecular analysis with molecular bands emission using laser-induced breakdown spectroscopy and chemometrics, *J. Anal. At. Spectrom.* 23 (2008) 694–701.
- [12] R.E. Russo, X. Mao, C. Liu, J. Gonzalez, Laser assisted plasma spectrochemistry: laser ablation, *J. Anal. At. Spectrom.* 19 (2004) 1084–1089.
- [13] R.E. Russo, X. Mao, S.S. Mao, The physics of laser ablation in microchemical analysis, *Anal. Chem.* 74 (2002) 70A–77A.
- [14] R.W. Bogue, Boom time for LIBS technology, *Sens. Rev.* 24 (2004) 353–357.
- [15] W. Pietsch, A. Petit, A. Briand, Isotope ratio determination of uranium by optical emission spectroscopy on a laser-produced plasma – basic investigations and analytical results, *Spectrochim. Acta Part B* 53 (1998) 751–761.
- [16] C.A. Smith, M.A. Martinez, D.K. Veirs, D.A. Cremers, Pu-239/Pu-240 isotope ratios determined using high resolution emission spectroscopy in a laser-induced plasma, *Spectrochim. Acta Part B* 57 (2002) 929–937.
- [17] H. Niki, T. Yasuda, I. Kitazima, Measurement technique of boron isotopic ratio by laser-induced breakdown spectroscopy, *J. Nucl. Sci. Technol.* 35 (1998) 34–39.
- [18] L. Mercadier, J. Hermann, C. Grisolia, A. Semerok, Plume segregation observed in hydrogen and deuterium containing plasmas produced by laser ablation of carbon fiber tiles from a fusion reactor, *Spectrochim. Acta Part B* 65 (2010) 715–720.
- [19] F.R. Doucet, G. Lithgow, R. Kosierb, P. Bouchard, M. Sabsabi, Determination of isotope ratios using Laser-Induced Breakdown Spectroscopy in ambient air at atmospheric pressure for nuclear forensics, *J. Anal. At. Spectrom.* 26 (2011) 536–541.
- [20] L.A. Kaledin, M.C. Heaven, Electronic spectroscopy of UO, *J. Mol. Spectrosc.* 185 (1997) 1–7.
- [21] M.C. Edelson, V.A. Fassel, Isotopic abundance determinations by inductively coupled plasma atomic emission spectrometry, *Anal. Chem.* 53 (1981) 2345–2347.
- [22] P.S. Goodall, S.G. Johnson, Isotopic uranium determination by Inductively Coupled Plasma Atomic Emission Spectrometry using conventional and laser ablation sample introduction, *J. Anal. At. Spectrom.* 11 (1996) 57–60.
- [23] M. Krachler, P. Carbol, Validation of isotopic analysis of depleted, natural and enriched uranium using high resolution ICP-OES, *J. Anal. At. Spectrom.* 26 (2011) 293–299.
- [24] R.C. Stern, B.B. Snavely, The Laser isotope separation program at Lawrence Livermore laboratory, *Ann. N. Y. Acad. Sci.* 267 (1976) 71–79.
- [25] B.W. Robertson, S. Adenwalla, A. Harken, P. Welsch, J.L. Brand, P.A. Dowben, J.P. Claassen, A class of boron-rich solid-state neutron detectors, *Appl. Phys. Lett.* 80 (2002) 3644–3646.
- [26] A.N. Caruso, P.A. Dowben, S. Balkir, N. Schemm, K. Osberg, R.W. Fairchild, O.B. Flores, S. Balaz, A.D. Harken, B.W. Robertson, J.L. Brand, The all boron carbide neutron detector: comparison with theory, *Mater. Sci. Eng. B* 135 (2006) 129–133.
- [27] J.P. Chaminade, O. Viraphong, F. Guillen, C. Fouassier, B. Czirr, Crystal growth and optical properties of new neutron detectors $Ce^{3+}:Li_6R(BO_3)_3$ ($R = Gd, Y$), *IEEE Trans. Nucl. Sci.* 48 (2001) 1158–1161.
- [28] K. Osberg, N. Schemm, S. Balkir, J.L. Brand, M.S. Hallbeck, P.A. Dowben, M.W. Hoffman, A handheld neutron detection sensor utilizing a new class of boron carbide diode, *J. IEEE* 6 (2006) 1531–1538.
- [29] R.F. Barth, D.E. Carpenter, A.H. Solloway, *Advances in Neutron Capture Therapy*, Springer, New York, 1993.
- [30] R.F. Barth, J.A. Coderre, M.J.H. Vicente, T.E. Blue, Boron neutron capture therapy of cancer: current status and future prospects, *Clin. Cancer Res.* 11 (2005) 3987.
- [31] D. Reed, The role of NMR in boron chemistry, *Chem. Soc. Rev.* 22 (1993) 109–116.
- [32] P. Bendel, Biomedical applications of ^{10}B and ^{11}B NMR, *NMR Biomed.* 18 (2005) 74–82.
- [33] B.J. Suh, X. Zong, Y. Singh, A. Niazi, D.C. Johnston, ^{11}B NMR in the layered diborides OsB_2 and RuB_2 , *Phys. Rev. B* 76 (2007) 144511–144514.
- [34] H.E. Goldbach, B. Rerkasem, B.A. Wimmer, P.H. Brown, M. Thellier, R.W. Bell, Boron in plant and animal nutrition, Springer, New York, 2002.
- [35] F.H. Nielsen, Boron in animal and human nutrition, *Plant Soil* 193 (1997) 199–208.
- [36] P.V. Ramachandran, H.C. Brown, Recent Advances in Borane Chemistry, ACS Symposium Series, Organoboranes for Syntheses, 783, American Chemical Society, Washington, DC, 2001, pp. 1–15, in Chapter 1.
- [37] B.S. Burnham, Synthesis and pharmacological activities of amine-boranes, *Curr. Med. Chem.* 12 (2005) 1995–2010.
- [38] C.C. Wang, S.A. Akbar, W. Chen, V.D. Patton, Electrical properties of high-temperature oxides, borides, carbides, and nitrides, *J. Mater. Sci.* 30 (1995) 1627–1641.
- [39] A.A. Bol'shakov, J.H. Yoo, C. Liu, J.R. Plumer, R.E. Russo, Laser-induced breakdown spectroscopy in industrial and security applications, *Appl. Opt.* 49 (2010) C132–C142.
- [40] Applied Spectra instruments, www.appliedspectra.com/products/.
- [41] A.I. Whitehouse, J. Young, I.M. Botheroyd, S. Lawson, C.P. Evans, J. Wright, Remote material analysis of nuclear power station steam generator tubes by laser-induced breakdown spectroscopy, *Spectrochim. Acta Part B* 56 (2001) 821–830.
- [42] B. Edlén, A. Ölme, G. Herzberg, J.W.C. Johns, Ionization potential of boron, and the isotopic and fine structure of $2s2p^2\ ^2D$, *J. Opt. Soc. Am.* 60 (1970) 889–891.
- [43] F. Mélen, I. Dubois, H. Bredohl, The A–X and B–X transitions of BO, *J. Phys. B* 18 (1985) 2423–2432.
- [44] Y.-K. Xiao, E.S. Beary, J.D. Fassett, An improved method for the high-precision isotopic measurement of boron by thermal ionization mass spectrometry, *Int. J. Mass Spectrom. Ion Processes* 85 (1988) 203–213.
- [45] G. Herzberg, Molecular spectra and molecular structure, I. Spectra of Diatomic Molecules, 2nd Ed., Van Nostrand Reinhold, New York, 1950.
- [46] J. González, C. Liu, J. Yoo, X. Mao, R.E. Russo, Double-pulse laser ablation inductively coupled plasma mass spectrometry, *Spectrochim. Acta Part B* 60 (2005) 27–31.